Chemical Engineering Journal 450 (2022) 138291

Contents lists available at ScienceDirect

Chemical Engineering Journal

journal homepage: www.elsevier.com/locate/cej

Neovascularization-directed bionic eye drops for noninvasive renovation of age-related macular degeneration

Meixin Ran [a,b,1], Yaxin Deng [a,1], Jiaqi Yan [b,1], Anan Zhang [a], Ying Wei [a], Xiaowen Li [a], Haibing He [a], Jingxin Gou [a], Tian Yin [e], Xing Tang [a], Jun Kong [d], Han Zhang [c,*], Hongbo Zhang [b,*], Yu Zhang [a,*]

[a] Department of Pharmaceutics, School of Pharmacy, Shenyang Pharmaceutical University Shenyang 110016, China
[b] Pharmaceutical Sciences Laboratory, Åbo Akademi University, Turku Bioscience Centre, University of Turku and Åbo Akademi University, Turku 20520, Finland
[c] Department of Ophthalmology, The First Hospital of China Medical University, Shenyang 110001, China
[d] Department of Ophthalmology Laboratory, The Fourth Affiliated Hospital of China Medical University Shenyang 110006, China
[e] School of Functional Food and Wine, Shenyang Pharmaceutical University, Shenyang 110016, China

ARTICLE INFO

Keywords:
Low-density lipoproteins
Age-related macular degeneration
Verteporfin
Penetratin
Eye drops

ABSTRACT

The current treatment of wet age-related macular degeneration (wAMD) relies on monthly intravitreal or intravenously injection of vascular endothelial growth factor (VEGF) inhibitor or photodynamic (PDT) agents to inhibit choroidal neovascularization. However, traumatic local therapy and exogenous long-distance fundus drug delivery often lead to secondary eye damage, low treatment efficiency, and immunogenic inflammation. Herein, inspired by the natural neovascular targeting ability of endogenous low-density lipoproteins (LDL), a noninvasive bionic nano-eye-drop with enhanced ocular penetrability and lesion recognizability is developed for enabling the PDT treatment of wAMD. Verteporfin (VP) as a laser-induced PDT agent is protected inside the hydrophobic core of reconstituted LDL (rLDL) vectors. 5-carboxyfluorescein (FAM) conjugated ste-penetratin (PEN, a transmembrane peptide) is anchored on the surface of the rLDL carrier, which enabled the nanoparticles (PEN-rLDL-VP) to cross the blood-retina barrier to realizing visual therapy. Following instillation, PEN-rLDL-VP can effectively deliver VP into neovascular that overexpress LDL receptors, which can respond to laser-induced PDT. Only with a single dose of the eye-drop and laser-induced PDT, the VEGF and proinflammatory intercellular adhesion molecule-1 (ICAM-1) proteins are significantly down-regulated *in vivo*, which implicates the neovascular inhibition and inflammation alleviation. This study presents an attractive non-invasive strategy for the PDT of wAMD.

1. Introduction

Many people over 60 years of age suffer from age-related macular degeneration (AMD) and endure irreversible vision loss [1]. It is estimated that there will be 300 million patients suffering from macular degeneration diseases by 2040[2]. Macular degeneration has two major types, the dry AMD and wet AMD, and the wet AMD (wAMD) condition is more severe [3,4]. wAMD is characterized by abnormal growth of new blood vessels into the choroid, followed by leakage or bleeding, causing vision-threatening scars in the macula [5]. wAMD is a multifactorial related disease, in which angiogenic factor (VEGF) plays an important pathogenic role in its pathological process [3,6].

Several treatments for AMD have been clinically implemented, such as laser coagulation, photodynamic therapy (PDT), radiation therapy, surgical therapy, and anti-vascular endothelial growth factor therapy [7]. To date, intravitreal injection of anti-VEGF drugs is the standard therapy for wAMD, however, it has been demonstrated as ineffective in reversing the existing neovascularization and patients would suffer from endophthalmitis and retinal detachment due to frequent injections [8]. Susvimo, formerly known as ranibizumab Port Delivery System, can continuously release ranibizumab, providing an alternative strategy to anti-VEGF eye injection for wet AMD patients. The routine monthly injection is improved to per six-month, that is, the implant is inserted into the eye through surgery and refilled every-six months. This product

* Corresponding authors.
E-mail addresses: zhanghan0614@139.com (H. Zhang), hongbo.zhang@abo.fi (H. Zhang), zhangyu@syphu.edu.cn (Y. Zhang).
[1] Meixin Ran, Yaxin Deng, and Jiaqi Yan contribute to this work equally.

https://doi.org/10.1016/j.cej.2022.138291
Received 18 May 2022; Received in revised form 19 July 2022; Accepted 21 July 2022
Available online 26 July 2022

can significantly improve the adaptability of patients, compared with once-a-month injection of anti-VEGF drugs, but it is still an invasive treatment. In addition, long-term inhibition of VEGF may also increase the risk of cardiovascular disease [9]. Therefore, a more efficient strategy with less damage, such as PDT, has received increasing attention for the treatment of wAMD. The effectiveness of PDT is attributed to the production of singlet oxygen by the photosensitizer after laser irradiation, resulting in platelet activation, thrombosis, and selective occlusion of the choroidal neovascularization (CNV) within the illuminated lesions [10,11]. At present, one of the PDT agents, verteporfin (VP), has already been approved by FDA for clinical treatment of AMD [12], which can stimulate the generation of short-lived singlet oxygen and oxygen free radical to terminate neovascular leakage, in response to non-thermal red light at a wavelength of 689 nm [13–15]. However, VP

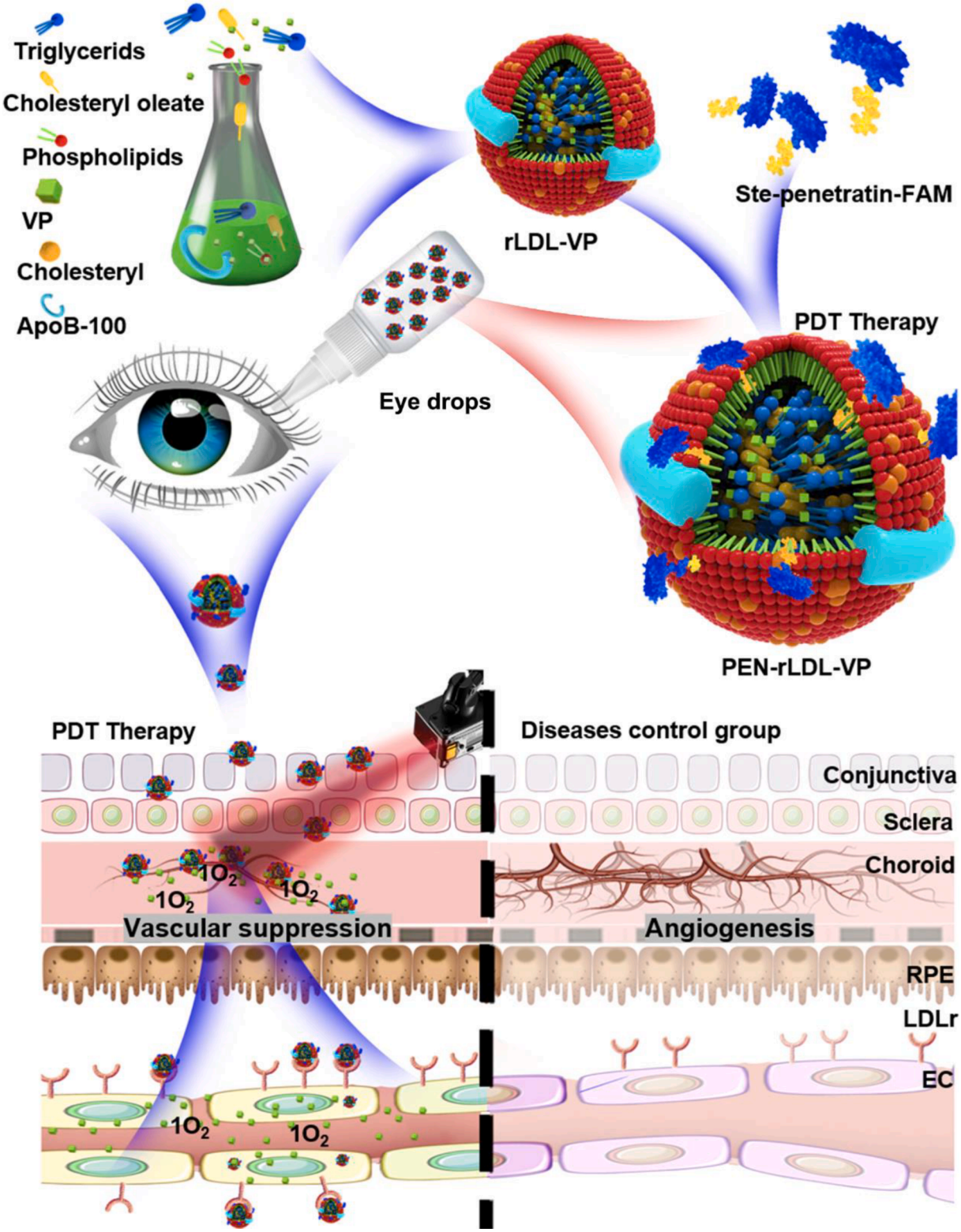

Fig. 1. Schematic representation for the composition of PEN-rLDL-VP and the treatment of wAMD after its topical application.

is currently administered intravenously, and this causes systemic phototoxicity with low delivery efficiency, which significantly hampers the use of VP for wAMD therapy.

As an endogenous substance, LDL has consisted of a lipid core and an apolipoprotein B-100 (ApoB), which has many unique advantages over synthetic materials, such as biocompatibility, the long half-life, biodegradability, and high drug loading capacity [16]. On the surface of neovascular endothelial cells, the LDL receptor is nearly 10 times overexpressed in comparison to normal endothelial cells [17–19]. LDL has been used to deliver anti-cancer drugs due to the accumulation of neovascular at the tumor site. Under wAMD conditions, the LDL receptor is also reported to overexpress in neovascular sites, but not in other healthy endothelial cells [20,21]. Therefore, LDL is a potential advanced carrier for targeted delivery of VP to posterior segment neovascularization for treating wAMD. Due to the limited availability of natural LDL and easily occurred infection during isolation of natural LDL, the reconstituted LDL is produced by microfluidization [22]. Reconstituted LDL (rLDL), with similar biological composition and structure to natural LDL, can be fabricated as promising vehicles for VP delivery [23].

Non-invasive ocular administration, such as eye drops [24], is the most tolerated treatment strategy for patients. Nevertheless, wAMD is a posterior segment disease in which drug delivery is severely challenged by the presented dynamic and static ocular barriers [25]. Cell-penetrating peptides (CPPs) are cationic peptide sequences, which are effective strategies for drug delivery as they can cross biological membranes and also carry carriers into cells. Penetratin possesses amphipathicity (the hydrophobic aromatic residues, 2 tryptophan and 1 phenylalanine) and PPII helix structure, which can be introduced to increase the drug penetration through static ocular barriers and to enhance the drug-delivering efficiency [26,27].

Herein, in this study, a low-density lipoprotein-inspired nanoparticle (PEN-rLDL-VP) was designed with high VP encapsulation efficiency and neovascularization recognizability for the targeted PDT of wAMD (Fig. 1). The effects of PEN-rLDL-VP on wAMD was investigated by cell experiments, intraocular distribution test, *in vivo* pharmacodynamic experiments, and *in vivo* biosafety evaluations. Due to the high biocompatibility of all contents within the PEN-rLDL-VP, it might serve as a promising strategy for clinical wAMD therapy, as well as for non-invasive drug administration to treat other types of fundus diseases.

2. Results and discussion

2.1. Preparation and characterization of PEN-rLDL-VP

To enhance the delivery efficiency and bioavailability, highly hydrophobic photosensitizer VP was protected inside bio-inspired reconstituted rLDL NPs, and the transmembrane peptide (PEN) was embedded

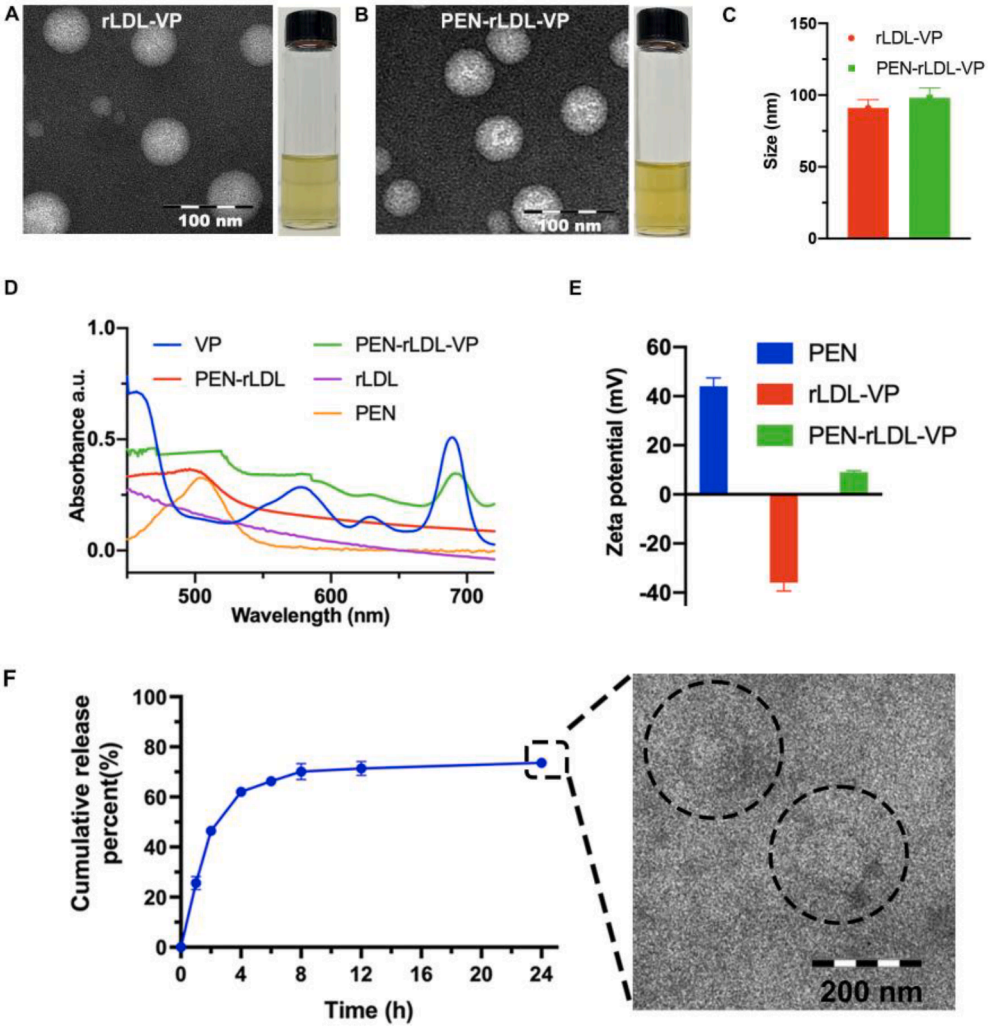

Fig. 2. Characterization of PEN-rLDL-VP. (A, B) Representative TEM images and photographs of rLDL-VP and PEN-rLDL-VP. Scale bars: 100 nm. (C) DLS size of rLDL-VP and PEN-rLDL-VP (n = 3). (D) visible spectrophotometry absorption spectra of VP, PEN, rLDL, PEN-rLDL, PEN-rLDL-VP. (E) Zeta potential of PEN, rLDL-VP, and PEN-rLDL-VP (n = 3). (F) Release profile of PEN-rLDL-VP and TEM image of nanoparticle broken (n = 3).

on the surface of rLDL to achieve ocular barrier penetration. We successfully prepared pure rLDL and VP encapsulated (rLDL-VP) NPs by emulsification-solvent evaporation method and optimum process parameters (Figs. S1, S2, S3) were determined: homogenization pressure (700 bar), homogenization times (4 times), and rotary steaming temperature (50 ℃). The screening principle of the prescription can be found in supplementary materials. The binding rate of Penetratin was determined by the fluorescence intensity measured with a microplate reader. The binding rate of penetratin was 60 %, indicating that penetratin was closely bound to the bionic nanoparticles to enhance the penetration of the nanoparticles into the eyes. The prepared rLDL and rLDL-VP NPs exhibited uniform sphericity with a size around 60 nm, as revealed by transmission electron microscopy (TEM) (Fig. S4, Fig. 2A). Meantime, the size of rLDL-VP observed from dynamic light scattering (DLS) was 91.2 ± 5.8 nm (Fig. S5), which might be caused by the absorption of the solvent molecules layer at the wetting stage [28–30]. Subsequently, we modified the PEN on the surface of rLDL-VP through electrostatic attraction (PEN-rLDL-VP). The PEN-rLDL-VP also exhibited uniform sphericity with a size around 60 nm in TEM (Fig. 2B) and AFM (Fig. S6), but with a DLS size of 98.5 ± 7 nm (Fig. 2C). In addition, as shown by the FTIR spectrum, a new peak was shown at 1650 cm^{-1} for PEN-rLDL-VP (Fig. S7) compared with the rLDL-VP group, which represented the N—H stretching vibration of modified PEN.

Subsequently, the drug loading and PEN modification were further verified by visible spectrophotometry, and the absorption spectra of VP, PEN, rLDL, PEN-rLDL, and PEN-rLDL-VP were shown in Fig. 2D. Compared with the rLDL group, the PEN-rLDL-VP group exhibited three VP characteristic peaks at 586 nm, 629 nm, and 691 nm, demonstrating that VP had been successfully loaded into the rLDL. The drug encapsulation efficiency and drug loading degree were 96.4 ± 1.6 % and 15.8 ± 0.5 mg/g (Table S1), which were calculated based on the equations S1 and S2 in the supplementary material. In addition, PEN characteristic peak at 503 nm was detected in PEN-rLDL and PEN-rLDL-VP groups by UV, which indicated that the amphiphilic PEN was embedded onto the surface of rLDL-VP NPs. Besides, zeta potential measurement was also utilized to prove the decoration of the cell penetration peptide PEN. The zeta potential of rLDL-VP NPs reversed from −36 mV to 9 mV after PEN modification, as shown in Fig. 2E. Hence, the PEN-rLDL-VP was successfully contrasted for further ocular drug delivery investigation.

To investigate the release of VP from the PEN-rLDL-VP, the PEN-rLDL-VP was incubated in simulated tear fluid at pH 7.4. The results showed that the NPs could release 75 % of loaded VP in 24 h (Fig. 2F). Furthermore, clear NP morphology change was observed in tear fluid, as no intact NP structure could be detected under TEM after the 24 h incubation (Fig. 2F), and the DLS data showed irregular size distribution (Fig. S5B).

2.2. Evaluation of the biocompatibility of pure nanocarrier and laser

Human umbilical vein endothelial cell (HUVEC cell) was selected as angiogenesis model cell and retinal pigment epithelial cell (ARPE cells) was chosen as the healthy cells. These two cell lines were treated with the pure carrier rLDL and PEN-rLDL NPs for another 48 h at different concentrations (0–2 mg/mL) after laser irridiation (Fig. S8A). Interestingly, for both rLDL and PEN-rLDL NPs, negligible toxicity was detected. Furthermore, different laser intensities (200–600 mW) were given to the HUVEC and ARPE cells. Again, negligible toxicity was detected in HUVEC cells and ARPE cells with further incubation for 48 h. (Fig. S8B). These results verified these bionic NPs possessed excellent biocompatibility and the laser power we selected was safe for the cells.

2.3. Evaluation of cell uptake

On the surface of neovascular endothelial cells, the LDL receptor is nearly 10 times overexpressed compared to normal endothelial cells. Therefore, LDL receptor-mediated enhanced endocytosis of our designed nanosystem could greatly facilitate the targeted delivery of VP to neovascularization. To verify the neovascular targeting of the nanoparticles, we blocked LDL receptors on the HUVEC surface for mimicking normal endothelial cells, and compare the endocytosis effects with normal HUVEC cells. ApoB, as a ligand for LDL receptors, is used to block LDL receptors, as shown in Fig. 3**A**. PEN (green) and VP (red) were used to track the NPs in cells.

For the rLDL-VP group, we found the uptake efficiency of NPs in normal HUVEC cells was around 3 times higher than in ApoB pre-saturated HUVEC cells. This indicated that ApoB could enhance the uptake of NPs through ApoB-mediated endocytosis, which was highly dependent on LDL receptors. Furthermore, for the PEN-rLDL-VP group, the uptake in the normal HUVEC cells was around 4 times higher than ApoB pre-saturated HUVEC cells, and the PEN-rLDL-VP group reflected higher uptake ability compared with the rLDL-VP group for ApoB-blocked HUVEC. Therefore, the rLDL system is a promising system for targeting the delivery of VP to neovascularization, and the modification of PEN could further enhance the uptake ability of NPs but did not change the LDL receptor-mediated uptake passway.

In addition, we also studied the colocalization of PEN with VP. As revealed in Fig. 3**B**, the red (VP) and green (PEN) fluorescence was overlapping and mainly located in the cytoplasm of HUVEC cells at 4 h, which indicated that the PEN stably anchored on the surface of rLDL-VP NPs at the early stage of cell uptake. While, the co-locolization rate (Pearson's R value) of PEN to VP dropped from 0.92 (4 h) to 0.81 (8 h) (calculated by the Coloc2 plugin in Image J), which reflects the shedding of PEN from the surface of the nanoparticles (Fig. S9).

Moreover, the uptake of rLDL-VP and PEN-rLDL-VP NPs by normal HUVEC cells was further studied by flow cytometry (Fig. 3C, D). Results quantitatively reflected the time-dependent uptake of rLDL-VP and PEN-rLDL-VP in HUVEC cells. The fluorescence intensity of the PEN-rLDL-VP group was 1.4 times higher than that of the rLDL-VP group (Fig. 3E), which is in good agreement with the confocal results.

2.4. Endosome escape of PEN-rLDL-VP

Subsequently, we performed an endosomal escape experiment [31] to verify the VP escape from lysosomes after laser irradiation via lysosomal rupture. Lysosome (green) and VP (red) were labeled in cells. For the PEN-rLDL-VP without Laser group, Pearson's R overlap rate of green and red fluorescence was 0.85 at 4 h. While, with laser, it reduces to 0.73 (Fig. S10 A, B, C) which indicated that excitation of the laser accelerates VP escape from the lysosome. For 24 h, Pearson's R value of PEN-rLDL-VP with Laser group dropped to −0.09, indicating that the VP could escape from the lysosome. However, the Pearson's R value at 24 h without laser treatment remained at around 0.68, which proved that laser is the main reason for the escape of lysosomes. Because the nanoparticles we designed did not possess the proton sponge effect, which cannot break lysosomes by changing the osmotic pressure in lysosomes, but only through the active oxygen generated by the laser.

2.5. In vitro phototoxicity evaluation

To investigate the phototoxicity of NPs on HUVEC cells and ARPE cells, MTT assays were carried out. After incubating the nanoparticles with cells for 6 h, the nanoparticles-contained medium was replaced, and laser was applied. Subsequently, the cells were further incubated for another 24 h or 48 h to better observe the effect of VP on the cells. For the HUVEC cell line, the PEN-rLDL-VP and rLDL-VP NPs groups under a laser dose of 600 mW for 5 min exhibited notable phototoxicity to HUVEC cells in a dose- and time-dependent manners (Fig. 3F, G). For the rLDL-VP + Laser group, 37.5 % and 18.7 % survival rates were observed at 24 h and 48 h respectively. Nevertheless, the PEN-rLDL-VP group showed more potent inhibition of HUVEC cells, the survival rate was 30.2 % and 10.2 % at 24 h and 48 h respectively. The results suggested that PEN-rLDL-VP and rLDL-VP upon NIR radiation significantly

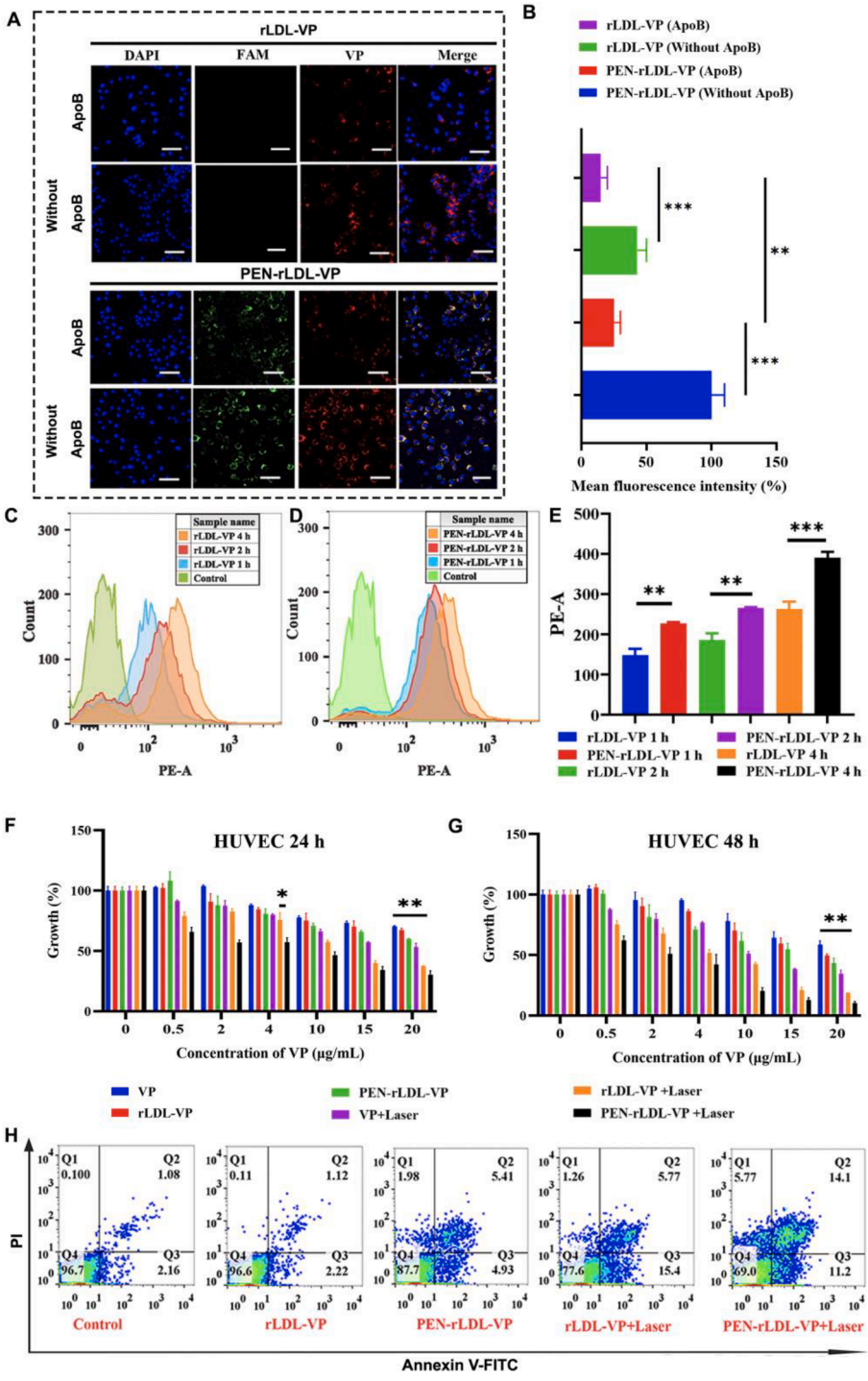

Fig. 3. (A) Confocal microscopy images and quantitative analysis of HUVEC cells taken at 4 h of PEN-rLDL-VP and rLDL-VP in the absence of laser with or without ApoB. (B) Quantitative analysis of HUVEC cells taken at 4 h of PEN-rLDL-VP and rLDL-VP in the absence of laser with or without ApoB. (Red represents the VP and green represents the PEN, n = 3). (C, D) Results of HUVEC cells uptake of rLDL-VP and PEN-rLDL-VP in the absence of laser-measured by flow cytometry. (E) Quantitative analysis of uptake. (* $P < 0.05$, ** $P < 0.01$, *** $P < 0.001$, n = 3) (F, G) MTT assay and cell apoptosis assay. Quantitative growth of HUVEC cells treated with varying VP concentrations (0, 0.5, 2, 4, 10, 15, 20 $\mu g \cdot mL^{-1}$) of VP drug, rLDL-VP and PEN-rLDL-VP (±Laser) for 24 h and 48 h, n = 3) (H) Cell apoptosis assay of rLDL-VP (±Laser) and PEN-rLDL-VP(±Laser) in HUVEC cells (VP, 4 $\mu g \cdot mL^{-1}$) after 6 h incubation. Cell apoptosis was analyzed by flow cytometry, n = 3.

inhibited the growth of HUVEC cells, and PEN modification promoted the inhibition effect. However, for ARPE cells, both of rLDL-VP + Laser and PEN-rLDL-VP + Laser groups were only slightly toxic to cells, and the survival rate of ARPE cells was over 80 % after 48 h (Fig. S8 C, D). These results indicated that this biomimetic nanosystem as an eye drop would not cause eye tissue damage, which is attributed to the high rLDL receptor targeting ability of PEN-rLDL-VP nanoplatforms for neovascularization.

Next, to examine the proapoptotic effect of PDT in HUVEC cells, the Annexin V/PI assays were also performed. We found that when laser excitation was lacking, the rLDL-VP and PEN-rLDL-VP groups did not have high toxicity and showed high safety and the apoptosis rates were 1.12 % and 5.41 %. However, with 5 min laser irradiation, and further incubation for 6 h, the rLDL-VP, and PEN-rLDL-VP NPs groups were programmed to undergo apoptosis, indicating that the system can realize NIR-mediated photodynamic therapy. Meantime, PEN promoted apoptosis of NPs and a higher curative effect (Fig. 3H) was found in PEN-rLDL-VP + Laser group (apoptosis rate, 14.10 %), compared with the rLDL-VP + Laser group (apoptosis rate, 5.77 %), which was consistent with the MTT assays. Taken together, these results proved the PEN-rLDL-VP could successfully deliver VP to HUVEC cells to produce the proapoptotic effect.

2.6. Intracellular $1O_2$ generation

Meantime, the generation of sufficient singlet oxygen ($1O_2$) in HUVEC cells is another critical factor responsible for the PDT effect. The capacity of intracellular $1O_2$ generation was investigated by the detection of a singlet oxygen sensor green (SOSG) probe at 525 nm for rLDL-VP and PEN-rLDL-VP with and without laser groups. The $1O_2$ shows in green in cells. From the results, we observed that without laser irradiation, all groups showed negligible $1O_2$ generation in cells. However, with laser irradiation, the PEN-rLDL-VP group showed the highest $1O_2$ generation ability, which increased by approximately 411 % (Fig. 4A, Fig. 4B) compared with no laser group. For the rLDL-VP + Laser group,

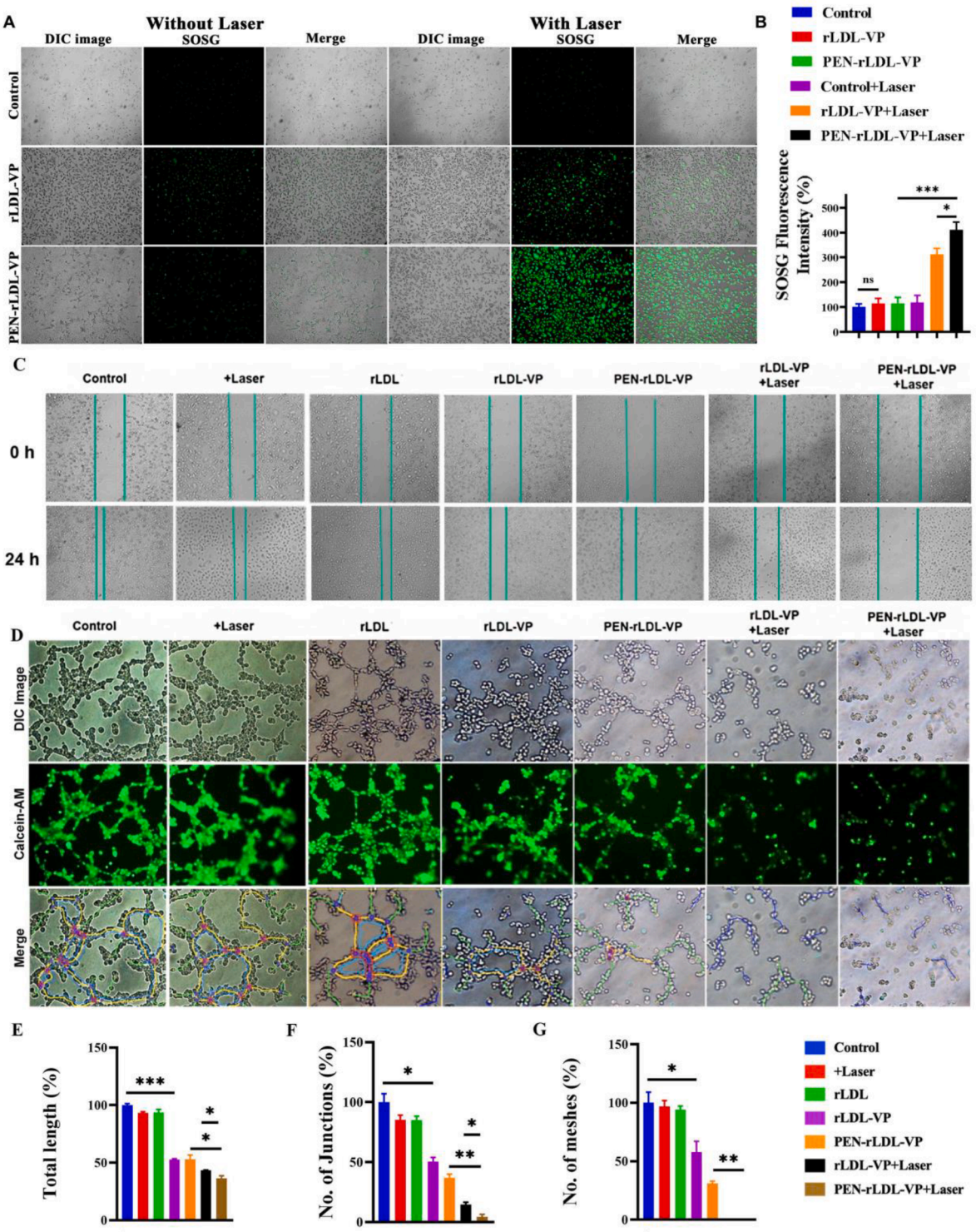

Fig. 4. (A) Intracellular $1O_2$ production from rLDL-VP and PEN-rLDL-VP (VP, 4 $\mu g \cdot mL^{-1}$) with and without laser. (B) Quantification of fluorescence intensity. (Green for singlet oxygen, n = 3) (C) Representative images of PEN-rLDL-VP (Laser, VP, 4 $\mu g \cdot mL^{-1}$) (D) Representative images of the total number of tubes per well tube formation on Matrigel at 8 h. The green line represents total length, the pink dots represent the junction, and the yellow circle represents the mesh. (E, F, G) Quantification of the total number of tubes per well, (E) total length, (F) number of junctions, (G)total number of meshes (* $P < 0.05$, ** $P < 0.01$, ***$P < 0.001$n = 3).

we observed the amount of $1O_2$ was only increased by 310 %. Thus, more $1O_2$ was produced in HUVEC cells in PEN-rLDL-VP with laser, and as a consequence, the presence of PEN could enhance the intracellular uptake and thus lead to more $1O_2$ generation in HUVEC cells.

2.7. Inhibition of HUVECs migration

Cell migration is a crucial process in angiogenesis, and the wound-healing assay is one of the commonly used assays for studying cell migration [32]. In this study, we measured the inhibition effects of different VP delivery systems (rLDL-VP and PEN-rLDL-VP NPs) on HUVEC cell migration after 24 h of drug administration, as shown in Fig. 4C and Fig. S11. The blank cells without any treatment were used as the control group. The results showed that rLDL-VP and PEN-rLDL-VP NPs groups without laser irradiation exhibited certain inhibitory effects (percent wound closure, 54.35 %, and 55.46 %) on the migration of HUVEC cells compared with the untreated control group (percent wound cloture, 81.92 %). More interestingly, rLDL-VP + Laser represented a more obvious effect on inhibiting cell migration (percent wound closure, 18.15 %) and PEN-rLDL-VP + Laser had the most significant inhibitory effect (3.70 %), probably due to the enhanced endocytosis of PEN-rLDL-VP.

2.8. Tube formation experiment

Tube formation ability of endothelial cells is another key factor in angiogenesis [33,34]. To explore the effects of NPs on angiogenesis inhibition, HUVEC cells were treated with rLDL-VP ± Laser and PEN-rLDL-VP ± Laser (4 μg/mL of VP) respectively (Fig. 4D). The total length, number of junctions, and total number of meshes were statistically analyzed with Image J software, and the results are shown in Fig. 4E-G. From the results, the HUVEC cells in the untreated control group, pure laser group, and pure rLDL group could form typical cord-like structures on the matrix gel and a large number of tubular structures with multiple branches were finally closed into tubes (Fig. 4D). Meantime, the rLDL-VP and PEN-rLDL-VP groups without laser had only a slight inhibition effect on tube formation, as compared with the control group, the total length was 52 ± 0.7 % and 53 ± 3.7 %, the number of junctions was 50 ± 3.3 % and 37 ± 3.0 %, and the number of meshes was 57 ± 9.1 % and 30 ± 2.1 %. With the laser, the rLDL-VP exhibited apparent inhibition in angiogenesis. The total length was 43 ± 0.2 %, the number of junctions was14 ± 1.9 % and the number of meshes was 0. More interestingly, the PEN-rLDL-VP + Laser group exhibited the strongest inhibition in angiogenesis. The total length was 36 ± 2.3 %, the number of junctions was 4 ± 1.9 % and the number of meshes was 0. The nanoparticle plus laser groups had inhibited the typical formation of tubular network structure, with a significant difference from the non-laser groups. This observation was in agreement with the wound-healing assay. Taken together, the activated PEN-rLDL-VP exhibited a significant effect on the angiogenic event of HUVEC cells.

The timepoint of tubule formation assays should consist with other tests including 24 and 48 h, however, due to the HUVEC cells start to undergo apoptosis after 24 h, and this leads to detachment from the matrix and the breaking of the tubes, only a short time point can be observed. In our case, during the observation, 8 h is the best timepoint that we can manage to capture the best tube formation phenomenon, hence, 8 h timepoint was choose for the observation of tube formation. At the same time, since the matrix gel had a certain thickness and was not completely flat, it was possible for cells to grow in different planes, so it was normal for some cells to be round in the photograph.

2.9. In vivo ocular distribution

In vitro studies have shown that rLDL, as an ideal bionic nanomaterial, had significant advantages for the LDL-mediated neovascular targeted delivery of VP, and it did not produce toxicity to healthy cells. Therefore, we further investigated whether the addition of the transmembrane peptide PEN promoted VP delivery from the ocular surface to the fundus, and the drug distribution of rLDL-VP and PEN-rLDL-VP NPs group in the eye. The VP contents in the conjunctiva, cornea, iris, retina-choroid, sclera, aqueous humor, lens, vitreous, and plasma were determined by LC-MS (Fig. 5A, Fig. S12). The area under the curve (AUC) of VP in retina-choroid tissue for the PEN-rLDL-VP treated group was around 9400 ng*h/g. However, in the rLDL-VP treated group only 3900 ng*h/g VP was detected, which confirmed the PEN modification greatly boosted the penetrability of the rLDL-VP NPs.

It is indeed very difficult for VP to penetrate and reach the retinal tissue through eye drop formulation, even with the PEN-rLDL-VP nanosystem, we only delivered 0.58 % of the original dose within 8 h, but this is already a quite big improvement compared with strategies from other Lab or even benchmark therapy. For instance, Bucolo et al. had carried out single instillation of Indomethacin in rabbit's eye and the $AUC_{0\text{-}4h}$ of 65496 ng*h/g were observed in retina, which means 0.1 % of the original dose reached the target tissue [35]. Meanwhile, our group has also conducted other nanosystems for the treatment of posterior segment diseases. The $AUC_{0\text{-}24h}$ in the retina-choroid was approximately 6000 ng*h/g with 50 μg single dose eye-drops, which means 0.12 % of the original dose reached the target tissue [36]. Besides, before the listed drug Visudyne® (vertiporfin liposome formulation) was put on the market, Gragoudas et al. used New Zealand White and Pigmented Rabbits to conduct preclinical pharmacokinetic study of vertiporfin liposome preparation in 1996 [37]. For 2 kg rabbits, the dosage was as high as 4 mg. From the perspective of pharmacokinetics, although the dosage was as high as 2 mg/kg, the $AUC_{(0\text{-}24h)}$ of retinal drugs studied by Gragoudas was 6,632 ng * h/g. If the weight of retinal tissue is usually 0.01 g, only 66.32 ng drugs were exposed to the retina, and the delivery efficiency is only around 0.001 % Therefore, this rLDL constructed biomimetic carrier was a great breakthrough for posterior segment drug delivery, which is logical to achieve promising results *in vivo*.

Moreover, we also observed that high VP levels were observed in the sclera and retina-choroid tissues (Fig. 5A, Fig. S13), while undetectable drug levels were observed in aqueous humor, lens, and vitreous humor. This may be because the surface area of the conjunctiva was 17 times bigger than that of the cornea [38,39] and the permeability can be as high as 29 times that of the cornea [40]. Also, nanocarriers with a diameter<300 nm could be easily absorbed by conjunctiva [40]. Meantime, the sclera, composed of collagen and elastin chains, is a porous membrane that allows the penetration of hydrophilic macromolecules. Therefore, we confirmed that the non-corneal (conjunctival/scleral) pathway was the primary pathway of nanoparticles to the posterior eye tissue, and both rLDL-VP and PEN-rLDL-VP NPs could effectively deliver drugs to posterior ocular tissues and treat posterior ocular diseases in a non-invasive manner.

Later, to determine the optimized time for laser irradiation treatment, the VP concentration was monitored at the retina-choroid by time and was plotted in Fig. 5B. As a result, the laser irradiation time for subsequent *in vivo* pharmacodynamics was set at 2 h after drug administration, since the highest drug concentration was detected.

2.10. PEN-rLDL-VP reduces vascular leakage and suppresses the formation of CNV

The laser-induced choroidal injury model (CNV) in mice was established and utilized for pharmacodynamic experiments. On the 21st day of CNV induction, mice were treated with rLDL-VP or PEN-rLDL-VP via topical instillation (16 μg VP, each eye) respectively. After 2 h, laser irradiation was performed (600 mW/cm^2 for 83 s)[41]. Abnormal vascular leakage is a sensitive indicator of wAMD. To examine the effect of PDT treatment with rLDL-VP and PEN-rLDL-VP eye drops on vascular leakage, fundus fluorescein angiography (FFA) examination was performed on CNV model mice on the 24th day (Fig. 5C).

From the results, the blood vessels in the healthy group were intact

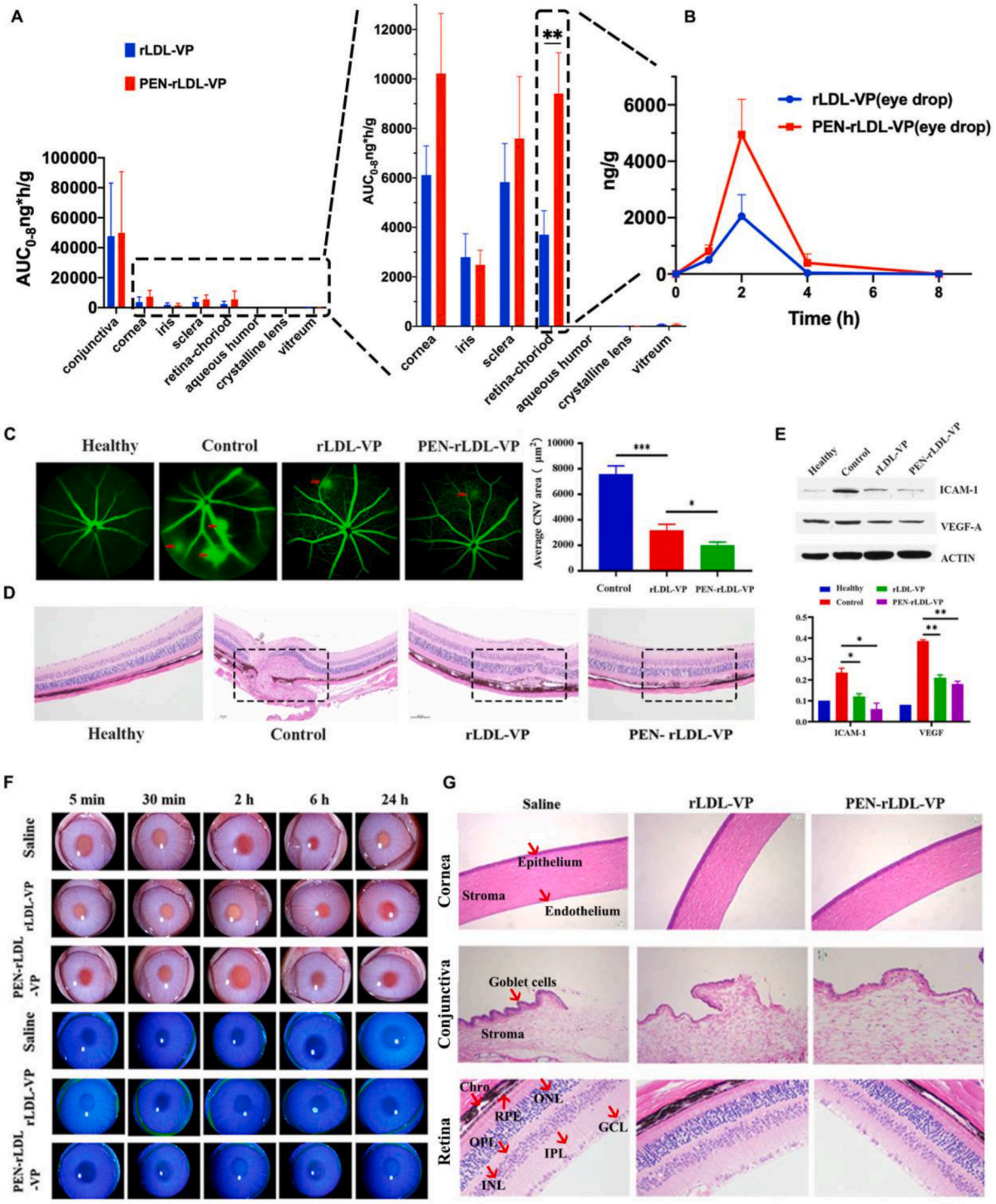

Fig. 5. (A) AUC of rLDL-VP-eye drop, PEN-rLDL-VP-eye drop, rLDL-VP-I.V., and PEN-rLDL-VP -I.V. in different ocular tissues (the results of the cornea, iris, sclera, retina-choroid, aqueous humor, crystalline groups were amplified and inserted, n = 3) (B) The mean VP concentration of rLDL-VP-eye drop, PEN-rLDL-VP-eye drop, rLDL-VP-I.V. and PEN-rLDL-VP-I.V. in retina-choroid. (C) Representative examples of fluorescence fundus angiograms from the healthy, the untreated, rLDL-VP, and PEN-rLDL-VP groups on the 24th day and quantification analyses of CNV areas on the 24th day. (* $P < 0.05$, *** $P < 0.001$, n = 3) (D) Images for retinal sections of experimental groups stained with HE on the 28th day (400 ×), n = 3. (E) The effect of rLDL-VP and PEN-rLDL-VP on the protein expression of VEGF and ICAM-1 in CNV disease models on the 28th day and quantification result of Western blot analysis by ImageJ software. (n = 3, * $P < 0.05$, ** $P < 0.01$) (F) Ocular irritation test for corneal injury in rabbits of saline, rLDL-VP, and PEN-rLDL-VP. (Cobalt blue light with fluorescein sodium). (G) Histological examination of the cornea, conjunctiva, and retina of saline, rLDL-VP, and PEN-rLDL-VP, n = 3.

and with no leakage. While, the blood vessels in the CNV model group had a lot of leakages (marked in red), with a leakage area of 7639 μm^2. After rLDL-VP + Laser treatment, the blood vessels were relatively repaired, and the leakage area was reduced to 3188 μm^2. More importantly, the vascular in the PEN-rLDL-VP group was remarkably repaired with only a slight leakage area of 1930 μm^2. Therefore, these results demonstrated that PEN-rLDL-VP could greatly reduce vascular leakage, and the PEN modification enhanced the photothermal

treatment effect of VP in the eyes.

Verteporfin is a highly effective photosensitizer, which could achieve significant vascular leakage inhibition within 24 h after a single dose of treatment [42]. What is more, in real clinical practice, the intravenous treatment cycle of the listed drug Visudyne® (verteporfin liposome) is once every-three months, which means single administration can achieve the treatment of wAMD. (Ultra-high drug doses and severe side effects including no visible natural light to the skin for 48 h, were the current clinical challenges, which are solved by this project.) Meanwhile, we had confirmed the highest drug concentration in retina tissue at a 2 h time point, therefore, the therapeutic effect was guaranteed.

H&E staining was also utilized to confirm the pharmacodynamics of our nanosystem, as shown in Fig. 5D. The retina and choroid tissues were clear and intact in normal healthy mice. However, the fundus structure was damaged in the CNV model, with edema and disordered cells in the photocoagulation area, spreading along with the entire retinal layer. In addition, in the CNV model, the pigment epithelial cells proliferated and migrated obviously, and the outer nuclear layer was damaged. These results once again prove the success established by the model.

Again, the nanoparticles can promote the renovation of CNV. In the rLDL-VP group, significantly reduced new vascular was observed in the retina and choroid region on the 28th day of CNV induction, and the retinal structure was clearer than in the CNV control group. More importantly, the PEN-rLDL-VP group was more effective. The retinal structures were well preserved, and the cells were arranged neatly after PEN-rLDL-VP treatment. The only small amount of fibroblasts proliferation and new vascular formation was detected on the 28th day of CNV induction. These results strongly proved that our penetrability enhanced PEN-rLDL-VP eye-drop possessed excellent retinal renovation ability.

2.11. PEN-rLDL-VP attenuates overexpression of VEGF and ICAM-1

In addition to the H&E staining, we further studied the therapeutic mechanism for rLDL-VP and PEN-rLDL-VP NPs, and all groups were treated with laser irradiation. Overexpression of angiogenic growth factor (VEGF) from RPE is the primary cause of CNV pathogenesis. In addition, pro-inflammatory and anti-inflammatory cytokines are also involved in the formation of CNV. Adhesion molecules such as ICAM-1 can increase vascular permeability by altering the extracellular matrix and play an important role in introducing macrophages/microglia into inflammatory tissues [43,44]. Therefore, the effect of PEN-rLDL-VP on inducing the expression of VEGF and ICAM-1 was investigated by Western Blot.

From the results, the VEGF and ICAM-1 expressions were 4.75 and 2.4 times in the CNV model group compared to the healthy group. Encouragingly, with rLDL-VP treatment, the expression levels of VEGF and ICAM-1 dropped nearly 50 % and 55 % on the 28th day of CNV induction. Notably, the expression levels of VEGF and ICAM-1 significantly decreased by 54 % and 70 % with PEN-rLDL-VP treatment, as shown in Fig. 5E. These results indicated that PEN-rLDL-VP can significantly inhibit the overexpression of VEGF and ICAM-1, which can induce neovascular inhibition and inflammation alleviation.

2.12. In vivo ocular irritation test

Eye drops are directly applied to the corneal surface, and eye irritation is, therefore, an important factor in the development and clinical application of eye drops [45]. Since the rabbit eyeball was very sensitive to external stimuli, the rabbit was selected as the research subject. The results of the multiple-dose irritation test (laser irritation) for saline, rLDL-VP and PEN-rLDL-VP groups were shown in Fig. 5F, and all groups were under laser irradiation.

According to Draize's evaluation [46], each evaluation score for three groups was 0 points, thus there was no corneal opacity, no congestion, no abnormal secretion, and no increase in tears. A detailed definition of Daize's evaluation can be found in supplementary materials. (TableS2 and Table S3) There was also no macroscopic evidence of irritation in the cornea and iris. Results of corneal injury examination with fluorescein sodium and TUNEL assays were shown in Fig. 5F and Fig. S14. The absence of green fluorescence indicated no damage to the cornea. In summary, both rLDL-VP and PEN-rLDL-VP groups were safe and did not irritate eyes.

Other than that, the sectioning results of multiple-dose stimulation experiments with rLDL-VP and PEN-rLDL-VP are shown in Fig. 5G. After topical administration, the eyeball was taken and sectioned for H&E staining. The normal saline group was used as the control group, and there were no visible abnormal changes in the cornea (epithelium, stroma, endothelium), conjunctiva (Goblet cells, stroma), and retina (GCL, IPL, inner plexiform layer, INL, inner nuclear layer, OPL, outer plexiform layer, ONL, outer nuclear layer, RPE, retinal pigment epithelium and Chro, choroid), and the morphology was complete after rLDL-VP and PEN-rLDL-VP administration. Furthermore, the clear structure of each layer and the absence of inflammatory cell infiltration indicated that the rLDL delivery system was biocompatible for ocular administration.

3. Conclusions

In summary, with high VP encapsulation efficiency, PEN enhanced penetrability as well as LDL receptor-mediated targeting ability, a novel bio-inspired eye-drop was successfully fabricated and characterized for the treatment of wet AMD by a noninvasive strategy. Our bionic eye drops have shown outstanding biocompatibility and effective therapeutic effects both in *vitro* and *in vivo*. We confirmed that the rLDL system is a promising platform for VP targeting delivery to neovascularization sites based on the LDL-mediated cell targeting endocytosis. Also, the PEN could effectively enhance the NPś penetrability and facilitate the VP delivery to the posterior segment of the eye through eye-drop administration. It was found that PEN-rLDL-VP NPs could reduce HUVEC cell migration and disrupt the capillary formation in the scratching and tube formation experiment. The laser-activated NPs exhibited rapid closure of new blood vessels and down-regulation of VEGF and ICAM-1 in the laser-induced choroidal injury model after 1-week treatment. Therefore, this bio-inspired PEN-rLDL-VP eye drop displays great potential in the treatment of wAMD, and this promising delivery system might serve as a noninvasive strategy for other fundus disease therapy. One limitation of this study was only one sex of animal were used for the study of biodistribution (male rabbit) and pharmacodynamic (female mice). Since AMD disproportionately affects females, wAMD bearing animals with different sex should be compared and analyzed separately in the following study.

4. Experimental section

4.1. Fabrication of rLDL-VP and PEN-rLDL-VP

Bio-inspired reconstituted LDL nanoparticles of verteporfin (rLDL-VP) were prepared by the emulsion-solvent volatilization method. First, phospholipid, glyceryl trioleate, cholesterol oleate, and cholesterol (molar ratio = 3: 2: 1: 1) and VP (15 mg) were added to the mixture of acetone and ethanol. Next, the synthetic peptide was dissolved into the sodium oleate contained Tris-HCl buffer solution (pH 8.05). Thereafter the peptide was added at 3 % of the total cholesterol (molar ratio). Then the organic phase and the aqueous phase were mixed (1:4, V/V) under high-shear mixing, and were subjected to high-pressure homogenization (Avestin, Canada). Eventually, organic solvents were then removed by rotary evaporation (Shanghai Ailang Instrument Co., ltd., China) at 50°C to produce rLDL-VP. Then, PEN (200 μg/mL) was added followed by vortexing for 1 min and incubating at 37 °C for 1 h to produce PEN-rLDL-VP.

4.2. Binding rate experiment of Penetratin

The formation of PEN-rLDL-VP was confirmed by centrifugal ultrafiltration, and the nanoparticles were prepared with FAM-labeled stepenetratin. PEN-rLDL-VP(1000 μL) was added into a 0.1 % Tween 80 pre-saturated ultrafiltration centrifuge tube (MW = 10 kDa) and centrifuged at 3000 r/min for 15 min in a high-speed refrigerated centrifuge. The ultrafiltrate at the lower layer was transferred to a 96-well plate with a black background. Fluorescence intensity was measured by a microplate reader (excitation wavelength Ex = 492 nm, and emission wavelength Em = 518 nm).

The binding percentage of penetratin in nanoparticles is calculated according to the following formula:

$$Bound\ penetratin\% = 1 - \frac{\text{Cultrafiltrate}}{\text{Ctotal}} \times 100\%$$

Cultrafiltrate is the concentration of penetratin in the lower ultrafiltrate.

Ctotal is the total concentration of penetratin added to the system.

4.3. Characterization of PEN-rLDL-VP

The morphology of the obtained PEN-rLDL-VP was documented by atomic force microscopy (cypher ES) and transmission electron microscopy (TEM, JEM-1200EX, JEOL ltd., Japan). Samples were negatively stained by 2 % Uranyl acetate. The sample solution of VP was prepared by dissolved in methanol and the UV–vis absorption value was determined between 200 and 800 nm. For PEN-rLDL and PEN-rLDL-VP determination, 100 μL of samples were dissolved in 1900 μL methanol and the UV–vis absorption value was measured between 200 and 800 nm. The lyophilized preparations were observed by Fourier transform infrared spectroscopy.

4.4. Release experiment

After centrifugation of 2 mL of the formulation, it was dispersed in 2 % Tween 80, simulated tear fluid, pH 7.4, in EP tubes at 37℃. Then, 1 mL was taken at 1, 2, 4, 6, 8, 10, 24, 36 and 48 h and absorbed at 430 nm.

4.5. Cell uptake (confocal microscopy)

HUVEC cells were seeded in a 24-well plate with crawling slides, and PEN-rLDL-VP and rLDL-VP were added after 24 h, respectively. The group without any treatment was set as the control group. After that, the serum-containing medium was discarded and the media FAM co-labeled formulation groups were added immediately and cultured for 4 h and 8 h, respectively. The concentration of VP was determined to be 4 $\mu g \cdot mL^{-1}$ in the cytotoxicity experiments. After removal of the medium, the slides were rinsed with 1 mL of PBS and fixed at 37C for 15 min with 0.5 mL of 4 % paraformaldehyde. Then washed twice with 1 mL of PBS, stained with 0.4 mL DAPI for 20 min, and twice with 1 mL of PBS. The uptake of nanoparticles by HUVEC cells was observed under an LSM710 confocal microscope. (German Carl Zeiss).

4.6. Cell uptake (flow cytometry)

HUVEC cells were seeded in 6-well plates with a cell density of 50 × 10^4 per well). In the absence of laser, HUVEC cells were added to rLDL-VP or PEN-rLDL-VP and cultured for 1, 2, and 4 h, respectively. Next, HUVEC cells were rinsed with PBS and centrifuged at 1500 rpm/min at low temperatures. HUVEC cells collected after centrifugation were dispersed in a flow tube with 500 μL and passed through a 200-mesh sieve. The samples were kept in the dark before analyzing. The average fluorescence intensity of VP (PE-A, Ex/Em 488/613 nm) and cell number of HUVEC cells were monitored by flow cytometry.

4.7. Intracellular Singlet Oxygen Detection

HUVEC cells were cultured in 24 well plates with 1 × 10^5 cells per well. When HUVEC cells reached 70–80 % fusion, they were treated with different groups and incubated at 37 °C for 4 h. After 4 h of culture, SOSG solution (5 μM) was added to the cell culture medium. The cells were then rinsed with fresh medium and the SOSG fluorescence signal excited at 488 nm was imaged under an FV3000 confocal laser scanning microscope. Image J software was used to conduct quantitative analysis on the signal analysis of SOSG, and the levels of $1O_2$ produced in cells under different experimental conditions were displayed.

4.8. Wound healing assays

HUVEC cells (1 × 10^5 cells per well) were seeded into 24-well plates and scraped into the confluent layer of HUVEC cells with the end of 1 mL pipette tips. The detached cells in the well were removed with excess PBS and then the HUVEC cells were incubated with the rLDL-VP ± laser (0.6 $J \cdot cm^{-2}$) and PEN-rLDL-VP ± laser (0.6 $J \cdot cm^{-2}$) samples diluted in the culture medium for 24 h. Scratches were observed at 0 and 24 h post-induction of injury under an XD-101 inverted microscope and the area without cells was measured using Image J software. The formula is as follows:

$$\text{Percent wound closure}(\%) = \frac{\text{migration distance of test group}}{\text{migration distance of control group}} \times 100\%$$

4.9. Tube formation assays

The ability to inhibit neovascularization was evaluated by the HUVEC tubule formation experiment. The Matrigel (BD 356234), 24-well plate, pipette and pipette tips were placed in the fridge at 4 °C and pre-cooled overnight. Pre-cooled Matrigel (0.5 mL) was quickly added to the plate and incubated at 37 °C for 30 min to allow gelation to occur. Cells were prepared after half an hour of gel spreading, and the cell concentration was finally adjusted to 6 × 10^4 cells/well with new medium. The cell suspension and formulation were mixed homogeneously (VP, 4 $\mu g\ mL^{-1}$). The 24-well plate was taken out of the incubator, and 1000 μL of cell culture medium was added to the vertical bottom of each well firstly, and then the mixed cell suspension and nanoparticles were added gently along the wall of the well. After 8 h, parameters of tube formation (total length, junction, mesh) were quantified by Image J software.

4.10. Intraocular distribution

Male Japanese white rabbits were purchased from Liaoning Changsheng Biotechnology Co., ltd. The animal experimentation was approved by the University Ethics Committee of Shenyang Pharmaceutical University (license number: CSE20201113). Thirty-two healthy male Japanese white rabbits were randomly divided into 2 groups for different treatments: Group A and B were treated with rLDL-VP nanoparticles or PEN-rLDL-VP nanoparticles via topical instillation (16 μg, VP, each eye) respectively. Then, the rabbits were sacrificed by air injection at 1, 2, 4, and 8 h after treatments, and the left and right eyes were immediately collected. After the ocular tissues (aqueous, lens, vitreous, cornea, palpebral conjunctiva, iris, retina-choroid, and sclera) were dissected and separated, they were accurately weighed and cut, and mixed with ultrapure water for a final volume of 2 mL. Then, steel grinding beads (diameter = 3 mm × 2, 4 mm × 2) were added to the tissue suspension and homogenized at a frequency of 60 Hz for 5 min with a tissue homogenizer (KZ-II Tissue homogenizer, Wuhan Servicebio Technology Co., ltd.). Methanol (1 mL) and internal standard solution (porphine, THP) were successively added to the mixture samples and vortexed for 2 min. After that, VP was extracted with ether (4 mL) for 10 min and centrifuged at 12000 rpm for 5 min. The organic phase (2 mL) was

aspirated and evaporated with nitrogen at 40 °C for later analysis by UPLC-MS/MS.

4.11. Establishment of CNV model and administration

All C57BL/6 female mice (three mice per group) were anesthetized with 85 mg/kg ketamine and 14 mg/kg thiazine by intramuscular injection, and mydriasis was performed using 10 g/L cyclosporine I (towering company, Japan) eye drops, and ofloxacin eye cream was applied rapidly to the eye surface to prevent the occurrence of cataracts. CNV was induced by laser photocoagulation with a 532 nm YG frequency-doubled laser (150 mV, 100 ms, 100 μm). The photocoagulation site was around the optic nerve, 1.5–2.0 PD away from the optic disc, and avoiding the large blood vessels. Three spots were applied to each eye. The morphological index for laser photocoagulation to reach the target was the occurrence of gasified foam (thick white foam with a light ring), which indicated the rupture of Brunch's membrane at the laser spot. If there was bleeding in the fundus after photocoagulation, which indicated vascular injury, the eye would be marked separately. On the 21st day of CNV induction, mice were treated with rLDL-VP nanoparticles or PEN-rLDL-VP nanoparticles via topical instillation (16 μg VP, each eye) respectively. After 2 h, laser irradiation was performed (0.6 $J{\cdot}cm^{-2}$).

4.12. Fluorescein angiography (FFA)

On the 24th day of CNV induction, fluorescein sodium (5 %, 0.1 mL) was injected intraperitoneally for fundus fluorescence imaging. The recording was started after 2 min, and the late phase was observed 6–8 min after the injection with a Small animal retina image system (Phoenix Technology Group, the U.S.A). The area of CNV was calculated using Image J software.

4.13. Histological examination

Mice were anesthetized and sacrificed on the 28th day of CNV induction. Then, the eyeballs in each group were harvested and fixed with 4 % paraformaldehyde for 24 h. Then, the retina sections were separated to perform paraffin sections for hematoxylin and eosin staining. The specimens were examined with a light microscope.

4.14. Western Blot

Mice were provided by the Experimental Animal Center of Shenyang Pharmaceutical University. This experiment followed the guidelines for the Care and Use of Laboratory Animals, and the ethical approval number was SYPU-IACUC-C2020-12–3-117. The mice were anesthetized and sacrificed, and their eyes were resected to separate the choroid on the 28th day. Then, protein expression levels were measured after retinal homogenization. Western blotting was performed using standard methods.

4.15. Histological examination

The rabbits were euthanized after the irritation test. Then, the eyeballs in each group were harvested and fixed with 4 % paraformaldehyde for 24 h. Then, the corneal and conjunctival tissue sections were separated to perform paraffin sections for hematoxylin and eosin staining. The specimens were examined with a light microscope.

Declaration of Competing Interest

The authors declare that they have no known competing financial interests or personal relationships that could have appeared to influence the work reported in this paper.

Data availability

Data will be made available on request.

Acknowledgments

This work was supported by Shenyang Science and Technology Talent Support Program [RC210447], the National Natural Science Foundation of China (82172086, 81871472), National Key R&D Program of China [2020YFE0201700], Research Fellow (Grant No. 328933), Solution for Health Profile (336355), and InFLAMES Flagship (337531) grants from Academy of Finland. Finland China Food and Health International Pilot Project funded by the Finnish Ministry of Education and Culture (No. 280M0052K1) Liaoning Revitalization Talents Program [XLYC1907111, XLYC1908031], Liaoning Province Doctoral Start-up Fund Program [2019-BS-226], Liaoning BaiQianWan Talents Program [(2020)78], Career Development Program for Young and Middle-aged Teachers of Shenyang Pharmaceutical University [ZQN2019004] and 'Dual Service' Program of University in Shenyang. Meixin Ran (CSC202207960005) and Jiaqi Yan (CSC202107960001) was sponsored by the China Scholarship Council.

Appendix A. Supplementary data

Supplementary data to this article can be found online at https://doi.org/10.1016/j.cej.2022.138291.

References

[1] J. Chen, L.E.H. Smith, Nat. Med. 18 (2012) 658–660.
[2] W.L. Wong, X. Su, X. Li, C.M.G. Cheung, R. Klein, C.-Y. Cheng, T.Y. Wong, Lancet Glob. Health 2 (2014) e106–e116.
[3] P. Mitchell, G. Liew, B. Gopinath, T.Y. Wong, Lancet 392 (2018) 1147–1159.
[4] J.-Z. Chuang, N. Yang, N. Nakajima, W. Otsu, C. Fu, H.H. Yang, M.P. Lee, A. F. Akbar, T.C. Badea, Z. Guo, A. Nuruzzaman, K.-S. Hsu, J.L. Dunaief, C.-H. Sung, Nat. Commun. 13 (2022) 374.
[5] T. Ayoub, N. Patel, J. R. Soc. Med. 102 (2009) 56–61.
[6] R.L. Sidman, J. Li, M. Lawrence, W. Hu, G.F. Musso, R.J. Giordano, M. Cardó-Vila, R. Pasqualini, W. Arap, Sci. Transl. Med. 7 (2015), 309ra165-309ra165.
[7] M. Ratner, Nat. Biotechnol. 32 (2014) 701–702.
[8] C. Liu, K. Jiang, L. Tai, Y. Liu, G. Wei, W. Lu, W. Pan, ACS Appl. Mater. Interfaces 8 (2016) 19256–19267.
[9] U. Testa, G. Pannitteri, G.L. Condorelli, J. Cardiovasc. Med. (Hagerstown) 9 (2008) 1190–1221.
[10] C. Chu, J. Yu, E. Ren, S. Ou, Y. Zhang, Y. Wu, H. Wu, Y. Zhang, J. Zhu, Q. Dai, X. Wang, Q. Zhao, W. Li, Z. Liu, X. Chen, G. Liu, Adv Sci (Weinh) 7 (2020) 2000346.
[11] X. Zhao, I. Seah, K. Xue, W. Wong, Q. S. W. Tan, X. Ma, Q. Lin, J. Y. C. Lim, Z. Liu, B. H. Parikh, K. N. Mehta, J. W. Lai, B. Yang, K. C. Tran, V. A. Barathi, K. H. Cheong, W. Hunziker, X. Su and X. J. Loh, *Advanced Materials*, **n/a**, 2108360.
[12] P. Nowak-Sliwinska, H. van den Bergh, M. Sickenberg, A.H. Koh, Prog. Retin. Eye Res. 37 (2013) 182–199.
[13] S.J. Bakri, P.K. Kaiser, Expert Opin. Pharmacother. 5 (2004) 195–203.
[14] A.L. Chin, S. Jiang, E. Jang, L. Niu, L. Li, X. Jia, R. Tong, Nat. Commun. 12 (2021) 5138.
[15] H.A. Collins, M. Khurana, E.H. Moriyama, A. Mariampillai, E. Dahlstedt, M. Balaz, M.K. Kuimova, M. Drobizhev, V.X.D. Yang, D. Phillips, A. Rebane, B.C. Wilson, H. L. Anderson, Nat. Photonics 2 (2008) 420–424.
[16] D. Sobot, S. Mura, S.O. Yesylevskyy, L. Dalbin, F. Cayre, G. Bort, J. Mougin, D. Desmaële, S. Lepetre-Mouelhi, G. Pieters, B. Andreiuk, A.S. Klymchenko, J.-L. Paul, C. Ramseyer, P. Couvreur, Nat. Commun. 8 (2017) 15678.
[17] C.S. Thaxton, J.S. Rink, P.C. Naha, D.P. Cormode, Adv. Drug Deliv. Rev. 106 (2016) 116–131.
[18] J. Tian, S. Xu, H. Deng, X. Song, X. Li, J. Chen, F. Cao, B. Li, Int. J. Pharm. 517 (2017) 25–34.
[19] N. Sabnis, A.G. Lacko, Ther Deliv 3 (2012) 599–608.
[20] R.Z. Renno, J.W. Miller, Adv. Drug Deliv. Rev. 52 (2001) 63–78.
[21] S. Michels, U. Schmidt-Erfurth, Semin Ophthalmol 16 (2001) 201–206.
[22] S. Hayavi, G.W. Halbert, Biotechnol. Prog. 21 (2005) 1262–1268.
[23] W. Li, J. Fu, Y. Ding, D. Liu, N. Jia, D. Chen, H. Hu, Acta Biomater. 96 (2019) 456–467.
[24] . Y. C. Kim, M. D. Shin, S. F. Hackett, H. T. Hsueh, R. Lima e Silva, A. Date, H. Han, B.-J. Kim, A. Xiao, Y. Kim, L. Ogunnaike, N. M. Anders, A. Hemingway, P. He, A. S. Jun, P. J. McDonnell, C. Eberhart, I. Pitha, D. J. Zack, P. A. Campochiaro, J. Hanes and L. M. Ensign, Nat. Biomed. Eng., 2020, **4**, 1053-1062.
[25] Q. Lyu, L. Peng, X. Hong, T. Fan, J. Li, Y. Cui, H. Zhang, J. Zhao, Biomaterials 270 (2021), 120682.

[26] C. Liu, L. Tai, W. Zhang, G. Wei, W. Pan, W. Lu, Mol. Pharm. 11 (2014) 1218–1227.
[27] Y. Wang, K. Xia, L. Wang, M. Wu, X. Sang, K. Wan, X. Zhang, X. Liu, G. Wei, Small 17 (2021) e2005578.
[28] J. Yan, X. Xu, J. Zhou, C. Liu, L. Zhang, D. Wang, F. Yang, H. Zhang, ACS Appl. Bio Mater. 3 (2020) 1216–1225.
[29] C. Liu, X. Xu, J. Zhou, J. Yan, D. Wang, H. Zhang, BMC Mater. (2020) 2.
[30] Y. Cheng, Y. Yu, Y. Zhang, G. Zhao, Y. Zhao, Small 15 (2019) 1904290.
[31] H. Luo, C. Huang, J. Chen, H. Yu, Z. Cai, H. Xu, C. Li, L. Deng, G. Chen, W. Cui, Biomaterials 279 (2021), 121194.
[32] M. Safonov, J. You, J. Lee, V.L. Safonov, D. Berman, D. Zhu, Eng. Regener. 1 (2020) 1–5.
[33] J. Yan, Y. Wang, M. Ran, R.A. Mustafa, H. Luo, J. Wang, J.H. Smatt, J. M. Rosenholm, W. Cui, Y. Lu, Z. Guan, H. Zhang, Small 17 (2021) e2100479.
[34] X. Zhao, Y. Liu, C. Shao, M. Nie, Q. Huang, J. Li, L. Sun, Y. Zhao, Adv Sci (Weinh) 6 (2019) 1901280.
[35] V. Agrahari, A. Mandal, V. Agrahari, H.M. Trinh, M. Joseph, A. Ray, H. Hadji, R. Mitra, D. Pal, A.K. Mitra, Drug Deliv. Transl. Res. 6 (2016) 735–754.
[36] R. Sun, A. Zhang, Y. Ge, J. Gou, T. Yin, H. He, Y. Wang, G. Zhang, J. Kong, L. Shang, X. Tao, Y. Zhang, X. Tang, Exp. Opin. Drug Deliv. 17 (2020) 1305–1320.
[37] R. Haimovici, M. Kramer, J.W. Miller, T. Hasan, T.J. Flotte, K.T. Schomacker, E. S. Gragoudas, Curr. Eye Res. 16 (1997) 83–90.
[38] E. Ramsay, E.M. Del Amo, E. Toropainen, U. Tengvall-Unadike, V.P. Ranta, A. Urtti, M. Ruponen, Eur. J. Pharm. Sci. 119 (2018) 83–89.
[39] B. Kong, L. Sun, R. Liu, Y. Chen, Y. Shang, H. Tan, Y. Zhao, L. Sun, Chem. Eng. J. (2022) 428.
[40] A. Enríquez de Salamanca, Y. Diebold, M. Calonge, C. García-Vazquez, S. Callejo, A. Vila, M.J. Alonso, Invest. Ophthalmol. Vis. Sci. 47 (2006) 1416–1425.
[41] D.N. Zacks, E. Ezra, Y. Terada, N. Michaud, E. Connolly, E.S. Gragoudas, J. W. Miller, Invest. Ophthalmol. Vis. Sci. 43 (2002) 2384–2391.
[42] M.H. Reinke, C. Canakis, D. Husain, N. Michaud, T.J. Flotte, E.S. Gragoudas, J. W. Miller, Ophthalmology 106 (1999) 1915–1923.
[43] B. Wang, P.K. Li, J.X. Ma, D. Chen, Invest. Ophthalmol. Vis. Sci. 59 (2018) 3630–3642.
[44] R.F. Mullins, J.M. Skeie, E.A. Malone, M.H. Kuehn, Mol. Vis. 12 (2006) 224–235.
[45] S. Zhu, L. Gong, Y. Li, H. Xu, Z. Gu, Y. Zhao, Adv. Sci. (Weinh) 6 (2019) 1802289.
[46] J. Xu, Y. Ge, R. Bu, A. Zhang, S. Feng, J. Wang, J. Gou, T. Yin, H. He, Y. Zhang, X. Tang, J. Control. Release 305 (2019) 18–28.